Available online at www.sciencedirect.com
SCIENCE DIRECT®
Journal of Sound and Vibration 289 (2006) 577–594
JOURNAL OF SOUND AND VIBRATION
www.elsevier.com/locate/jsvi

Scattering and absorption of sound at flow duct expansions

S. Boij[a,*], B. Nilsson[b]

[a]*MWL, Department of Aeronautical and Vehicle Engineering, Kungl Tekniska Högskolan, SE-10044 Stockholm, Sweden*
[b]*School of Mathematics and Systems Engineering, Växjö University, SE-35195 Växjö, Sweden*

Received 27 June 2002; received in revised form 23 December 2004; accepted 15 February 2005
Available online 19 April 2005

Abstract

The scattering of plane acoustic waves at area expansions in flow ducts is analysed using the vortex sheet model where the flow at the expansion is modelled as a jet, with a vortex sheet emanating from the edge. Of particular interest is the influence of the flow field on acoustic scattering and absorption.

First, it is demonstrated that the stability properties of the shear layer can be simulated by modifying the edge condition within the vortex sheet model. To this end the accuracy for the region where the shear layer is changing from unstable to stable is improved by introducing a gradually relaxed Kutta edge condition with empirically derived coefficients. For low Strouhal numbers the vortex sheet model applies and for higher Strouhal numbers the two models converge.

Second, it is demonstrated that the acoustic transmission through the jet expansion region can be determined by neglecting the scattering there. Incorporating this assumption, the vortex sheet model reproduces well the experimental results on transmission and absorption for an area expansion. This result supports the assumption that the main part of the scattering occurs at the area expansion at least for the low-frequency range. Furthermore, the influence of the flow field is particularly strong for small Strouhal numbers.

1. Introduction

The physics of sound waves encountering thin shear layers in confined or free flows is in general very complex, and the flow–acoustic interaction sometimes has a significant influence on the

*Corresponding author. Tel.: +46 8 790 91 88; fax: +46 8 790 61 22.
E-mail address: sboij@kth.se (S. Boij).

0022-460X/$ - see front matter © 2005 Elsevier Ltd. All rights reserved.
doi:10.1016/j.jsv.2005.02.017

sound propagation. In particular, the interaction is considered to be strong at points of flow separation. A case of interest where these phenomena should be considered is the acoustics of sudden area expansions in flow ducts, where the flow separates at the sharp edge and a free shear layer emanates from the edge of the expansion.

When sound waves propagate through a moving fluid, the acoustic field and the mean flow field are often treated as two separate, non-interacting systems. Consider now models aiming at describing the acoustic field in the presence of a mean flow field including, e.g. flow separation. To include any significant interaction with the mean flow field, the model should include the corresponding coupling mechanisms of the flow–acoustic interaction. However, it is possible to neglect details of the steady flow that has a negligible influence on the acoustics. From the acoustical viewpoint, it is then important to know what the main coupling mechanisms are and when the interaction is strong enough to require consideration.

In this paper, a sound propagation model including flow–acoustic coupling occurring at the sharp edge of a sudden area expansion in a flow duct is investigated. The model, presented earlier by Boij and Nilsson [1], is an analytical model treating scattering at the sharp edge depicted in Fig. 1, where the scattering properties of an area expansion are derived by means of a building block method. The flow downstream of the interior splitter plate is modelled by means of a vortex sheet. In order to get a unique solution, the amount of vorticity shed is fixed by applying the classical unsteady Kutta condition [2] at the edge. This edge condition then provides a coupling mechanism between the acoustic field and the mean flow field, in particular the vortex shedding at the trailing edge. The acoustic scattering coefficients at the area expansion are derived with Wiener–Hopf methods, but the effect of the mean flow expansion is not included in the model.

A physical property of a free shear layer is that it is unstable in a certain parameter range, where the shear layer is thin in comparison to the wavelength of the disturbances. Thus, acoustic disturbances trigger the instability, i.e., the onset of vorticity shedding at the edge, this mechanism providing a possible coupling between the acoustic and the remaining flow field. In case this is the main coupling phenomenon, it ought to be included in the model. The fact that the vortex shedding occurs at the very location of the sharp edge indicates that it is important to have a proper modelling of the overall field at this point, and several works indeed point to the importance of a correct modelling of the flow field close to the edge [2].

In the Boij and Nilsson model, the flow–acoustic coupling is accounted for by the application of the Kutta condition at the sharp edge. Any coupling caused by the acoustic waves encountering the jet expansion region downstream of the duct expansion is neglected, as is the influence of the mean flow profile in this area. Originally, the model is intended for more complex duct elements, where a trailing edge is close to a leading edge. However, the promising results for the reflection properties of an area expansion inspired to investigate if the model is more general than first

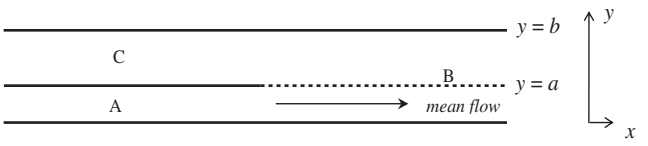

Fig. 1. Duct geometry for a trailing edge, where the dotted line represents the vortex sheet.

expected. In particular, the prediction of Strouhal number dependent phenomena indicate that flow–acoustic coupling is indeed covered by the model. With the practical applicability of the model in mind, we study the range of validity of our model from two aspects.

In the first part of the paper, we discuss the possibility of extending the theory to higher Strouhal numbers (loosely speaking, higher frequencies). In the present model, the shear layer is assumed to be infinitely thin, which makes the instability inherent in the model. This neglects the physical property that a shear layer becomes stable above a certain ratio between the thickness of the layer and the wavelength of the sound waves. Thus, the original model is restricted to the parameter region where the emanating shear layer is unstable to incoming sound waves [3]. By modifying the edge condition, we suppress the unstable part of the flow field downstream of the duct, while keeping the modelling of the shear layer as a vortex sheet. We propose a method to extend the valid range of the model to include both the region of transition from an unstable to a stable shear layer and the region of stable shear layers. A comparison with experimental results is included.

In the second part of the paper, the results for the acoustic field in the duct downstream of the expansion is investigated and compared with experimental results. The transmission and absorption of plane waves incident on an area expansion are studied, in order to evaluate the influence of the jet expansion and the mean flow profile, both neglected in the model. This is an issue of practical importance, as dissipation of sound influences the performance of silencers, and a better understanding of the physics would provide tools to improve the design.

The theoretical results are compared to experimental data found in Ref. [4]. It should be noted that the model is for a two dimensional, rectangular duct while the measurements are performed on a cylindrical geometry. In order to compare these two cases, a frequency scaling based on the first cut-on frequency of the wider duct is applied. This scaling is described in Ref. [1].

It should be mentioned that the vortex sheet model is well suited for analysis of more complex duct elements. This may be perforated plates or side branch apertures in a duct wall, i.e., apertures with grazing flow. The scattering properties of the leading edge involved in such geometries are described in Ref. [5].

2. Influence of conditions at the edge

2.1. Flow model

In the Boij and Nilsson model [1], the assumption for the steady flow at the edge is that the flow leaves the plate parallel to the plate surface, and that a vortex sheet emanates from the edge. The fluid velocity model is in accordance with the Kutta condition for steady flows. To get a unique solution for the unsteady acoustic field, the unsteady Kutta condition is applied at the edge. This condition, as well as that for the steady flow, prescribes that the velocity of the flow field remains finite at the edge. The application of the unsteady Kutta condition and alternative conditions is further discussed below.

The model does not include that the shear layer may be stable. A free shear layer is unstable for small Strouhal numbers; this is the case in the vortex sheet model. For large Strouhal numbers, the shear layer is stable; an effect that is not included by a vortex sheet with zero thickness, as the

infinitely thin vortex sheet is unstable for all frequencies. It is the effect of the stable region for the shear layer that we want to include in the model in order to see if it has any significant influence on the result. This is done by controlling the amplitude of the instability modes rather than changing the actual thickness of the shear layer in the model.

2.1.1. The instability of the shear layer

Consider the case of a semi-infinite plate, ending in a sharp trailing edge. On one side, the fluid is moving at a constant velocity parallel to the plate, and on the other side, the fluid is stagnant. Then a shear layer forms at the edge of the plate, a shear layer that is unstable to disturbances of low frequency. This so-called Kelvin–Helmholtz instability can be described as a vortex wave excited at the edge, growing exponentially as it propagates downstream [3]. The growth will be limited after a certain distance, in part by nonlinear phenomena.

It is the relationship between the thickness of the boundary layer and the wavelength of the incident sound wave that determines whether the shear layer is stable or unstable at the edge where the interaction between sound and flow is expected to take place. The shear layer Strouhal number is the parameter that governs the instability [6], and is denoted

$$St_\theta = \frac{k\theta}{M}, \tag{1}$$

where θ is the momentum thickness of the boundary layer just downstream of the inlet edge [7]. The Mach number in the duct part A is denoted M and the acoustic wavenumber k. The change from an unstable to a stable shear layer occurs around a critical value of St_θ. Freymuth [6] and Michalke [8] present experimental and theoretical results for the properties of free shear layers. They show that for a thin shear layer this critical Strouhal number is $St_\theta \approx 0.25$, while other authors report higher values [9]. Below the critical Strouhal number, the shear layer is unstable and for larger Strouhal numbers, the shear layer is stable.

To estimate when the vortex sheet model becomes unphysical, we need to relate this critical Strouhal number to the theoretical results. As the shear layer in the model has zero thickness, it is a low-frequency approximation and St_θ is zero. However, when it is possible, as for the experimental data used here, it is convenient to relate the finite thickness θ of the shear layer to the duct width. For the experimental data used in this paper [4], the flow in the duct is fully turbulent and the Reynolds number is of the order 10^5. The velocity profile for such a flow in a rectangular duct and for the parameters in this article, gives a boundary layer momentum thickness at the edge that is approximately 10% of the radius of the duct of this experiment. For the experimental data in this article, the shear layer Strouhal number St_θ is proportional to

$$St_a = \frac{ka}{M}, \tag{2}$$

where a is the width of the upstream duct. The critical Strouhal number is then $St_a \approx 2.5$. In the following, St_θ denotes the physical Strouhal number given by the current model parameters.

2.2. A variable edge condition

Now, we want to modify the vortex sheet model to take into account both stable and unstable shear layers, as suggested in Ref. [10]. This is done without changing the geometry of the model, in

this case the thickness of the shear layer. Instead, we want to simulate the influence of a shear layer of finite thickness by changing some other parameters. The stability properties of the shear layer are primarily described by the Strouhal number (based on the shear layer thickness). Based on this, we look for a way to simulate the stability properties as a function of the Strouhal number.

Indeed, the solution method provides a mathematical possibility to control the scattering amplitude of the instability wave. Such a procedure, presented below, involves a change of the edge condition, which originally is the unsteady Kutta condition. However, there are also physical arguments for such a change, as the unsteady Kutta condition is not valid for large Strouhal numbers. The starting point for the simulation of the Strouhal number dependent instability is to study the relation between the edge condition and the excitation amplitude of the instability wave, i.e., the growing hydrodynamic wave in the duct downstream of the edge. When St_θ is small and the shear layer is unstable to the disturbances caused by the sound wave, the unsteady Kutta edge condition is applicable [8]. For large St_θ, the shear layer is stable and is appropriate to use a different condition, suppressing the instability. By changing the edge condition, or rather the scattering amplitude of the unstable mode, the stability of the solution can be controlled.

The change from an unstable to a stable shear layer occurs around the critical value of St_θ [8]. Around this value, there exists a transition region where some kind of gradual change from the unstable to the stable solution would be appropriate. This is achieved by gradually decreasing the excitation of the instability wave with increasing Strouhal number. When the excitation of the unstable mode is fully removed, the solution contains no growing modes. Thus, we have related the edge condition to the excitation of the instability wave. Therefore, the condition which yields the stable solution is denoted the *relaxed Kutta condition*, and is derived in the next section.

2.2.1. Derivation of scattering coefficients, formulation and solution of the scattering problem

The edge condition enters the analysis when the scattering at the edge depicted in Fig. 1 is to be determined. The scattering problem is formulated as a Wiener–Hopf equation in Fourier space. For the formulation, we use Jones' method [11], where the Fourier transform is applied directly to the differential equations as well as boundary and coupling conditions.

First, we give a review of the necessary relations used in the analysis. Important in the Wiener–Hopf technique is the dispersion relation for duct B,

$$G(\alpha) \equiv \frac{\cot h(b-a)}{h} + (1 - M\alpha/k)^2 \frac{\cot Ha}{H} = 0, \tag{3}$$

where $H = \sqrt{(k - M\alpha)^2 - \alpha^2}$, $h = \sqrt{k^2 - \alpha^2}$ and b is the width of the downstream duct. The zeros of the dispersion relation represent the wavenumbers in duct B. The wavenumbers in ducts A and C are given by the ordinary dispersion relations for acoustic waves in ducts with a constant mean or no flow. The wavenumbers are denoted $\alpha^{\pm}_{Xn}$, representing the wavenumber of mode n in duct X, propagation in the $+/-$ (right/left) direction (Fig. 1). We also need the general modal function related to the mode shapes in all three duct parts (Fig. 2),

$$\begin{aligned} \varphi(\alpha, y) &= -\frac{(1 - M\alpha/k)^2 \cos Hy}{Ha \sin Ha}, \quad 0 < y < a, \\ &= \frac{\cos h(b-y)}{ha \sin hc}, \quad a < y < b. \end{aligned} \tag{4}$$

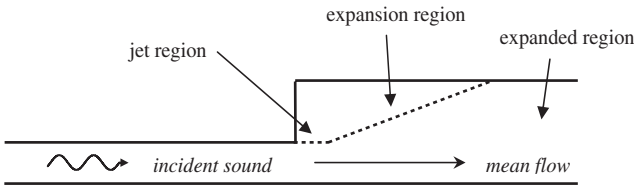

Fig. 2. A schematic picture of the expansion of the jet, where the flow is divided into three different regions and the dotted line indicates the shear layer.

The explicit expressions for wavenumbers and mode shape functions are given in the Appendix. In general, the acoustic pressure $p(x, y)$ in a duct can be expressed as a sum,

$$p(x,y) = \sum_n P_n^+ \varphi_n^+(y)\, \exp(\mathrm{i}\alpha_n^+ x) + \sum_n P_n^- \varphi_n^-(y)\, \exp(\mathrm{i}\alpha_n^- x). \tag{5}$$

Here, $P_n^\pm$ are the modal amplitudes, $\varphi_n^\pm$ are the mode shape functions and $\alpha_n^\pm$ are the axial wavenumbers of the nth mode respectively. For the different duct parts appearing in this problem, expressions for the modal amplitudes and for the mode shape functions are given in the Appendix. We can now define the Fourier transform as

$$P(\alpha, y) = P_+(\alpha, y) + P_-(\alpha, y) \equiv \int_{-\infty}^{0} p(x,y)\mathrm{e}^{-\mathrm{i}\alpha x}\,\mathrm{d}x + \int_0^{\infty} p(x,y)\mathrm{e}^{-\mathrm{i}\alpha x}\,\mathrm{d}x. \tag{6}$$

The Fourier transformed pressure $P(\alpha, y)$ can be expressed [5] in terms of the general mode shape function $\varphi(\alpha, y)$ and the function

$$\phi_-(\alpha) \equiv \frac{\partial P_-}{\partial y}(\alpha, a^+), \tag{7}$$

which is proportional to the displacement of the vortex sheet. The Fourier transformed pressure is then

$$P(\alpha, y) = a\varphi(\alpha, y)\phi_-(\alpha). \tag{8}$$

From the definitions above, a Wiener–Hopf equation for waves incident from ducts A and C, respectively, can be derived, yielding

$$G(\alpha)\phi_-(\alpha) + J_+(\alpha) + \frac{\mathrm{i}\varphi_{Am}(a)}{\alpha - \alpha_{Am}^+} - \frac{\mathrm{i}\varphi_{Cm}(a)}{\alpha - \alpha_{Cm}} = 0. \tag{9}$$

The third term in this equation represents a wave incident from duct A with modal amplitude set to one, and the fourth term similarly represents a wave with modal amplitude one, incident from duct C. The function $J_+(\alpha)$ is the pressure difference across the bifurcated duct, given by

$$J_+(\alpha) = P_+(\alpha, a^-) - P_+(\alpha, a^+). \tag{10}$$

The solution ϕ_- to Eq. (9) represents a right-going wave to the right of the plate edge. This property, interpreted as $\phi_-(\alpha)$ being regular in the lower α-plane, is central for solving the

Wiener–Hopf equation (9). To this end, the Wiener–Hopf kernel,

$$G(\alpha) = G_+(\alpha)G_-(\alpha), \tag{11}$$

is factorised such that G_+ is regular and non-zero for $\mathrm{Im}(\alpha) > \tau_-$ and G_- is regular and non-zero for $\mathrm{Im}(\alpha) < \tau_+$. Eq. (9) is now rearranged to give

$$G_-(\alpha)\phi_-(\alpha) + \frac{\mathrm{i}\varphi_{Am}(a)}{G_+(\alpha^+_{Am})(\alpha - \alpha^+_{Am})} - \frac{\mathrm{i}\varphi_{Cm}(a)}{G_+(\alpha_{Cm})(\alpha - \alpha_{Cm})} = Q(\alpha), \tag{12}$$

where Q is an unknown polynomial in α. The solution to this equation is given by

$$\phi_-(\alpha) = \frac{1}{G_-(\alpha)}\left[\frac{\mathrm{i}\varphi_{Cm}(a)}{G_+(\alpha_{Cm})(\alpha - \alpha_{Cm})} - \frac{\mathrm{i}\varphi_{Am}(a)}{G_+(\alpha^+_{Am})(\alpha - \alpha^+_{Am})} + Q(\alpha)\right] \tag{13}$$

2.2.2. Edge condition

In order to determine the polynomial Q, thus achieving a unique solution to the Wiener–Hopf equation, an additional condition is required. It is at this stage in the analysis that the edge condition is applied. For parameters corresponding to thin shear layers, i.e., small St_θ below the critical value, the appropriate choice is the unsteady Kutta condition for a trailing edge. It prescribes that the velocity of the fluid along the plate remains finite at the edge [5]:

$$\frac{\partial p}{\partial y}(x, a^+) = O(x^{3/2}) \quad \text{when } x \to 0^+. \tag{14}$$

This edge condition requires that $Q(\alpha) = 0$ in Eq. (12), which implies a unique solution.

Now, if the polynomial $Q(\alpha)$ is instead chosen to have degree zero, i.e., Q is any non-zero constant independent of α, the solution will instead satisfy the acoustic, no flow edge condition,

$$\frac{\partial p}{\partial y}(x, a^+) = O(x^{1/2}) \quad \text{when } x \to 0^+, \tag{15}$$

which allows for a singularity in the velocity at the edge. As this holds for general constants Q, this choice allows for some further modelling. To model the dynamics of a stable shear layer, we chose Q so that the amplitude of the instability wave is set to zero. Thus, in the small St_θ region, Q is chosen to be zero, in accordance with the original Kutta condition (14). In the region of large St_θ, Q is instead chosen so that the scattering coefficient for the growing hydrodynamic mode is zero in order to suppress the excitation of this mode. A Strouhal number dependent coefficient, varying between zero and one, is chosen so that the excitation of the instability decreases gradually with increasing St_θ. With the subscript gr indicating the growing hydrodynamic mode, Q is then given by

$$Q(\alpha) = A(St_\theta)\left(-\frac{\mathrm{i}\varphi_{Cm}(a)}{G_+(\alpha_{Cm})(\alpha_{B,\mathrm{gr}} - \alpha_{Cm})} + \frac{\mathrm{i}\varphi_{Am}(a)}{G_+(\alpha^+_{Am})(\alpha_{B,\mathrm{gr}} - \alpha^+_{Am})}\right), \tag{16}$$

where the complex valued coefficient A,

$$0 \leqslant |A(St_\theta)| \leqslant 1. \tag{17}$$

As described above, $A = 1$ corresponds to the case when the excitation of the growing hydrodynamic wave is prescribed to be zero. In the transition region, where the shear layer changes from unstable to stable, the coefficient $A(St_\theta)$ should gradually increase from 0 to 1.

To retrieve the spatial pressure field $p(x, y)$, we take the inverse Fourier transform of relation (8) with the expression in Eq. (12) inserted. This yields

$$p(x,y) = \frac{\mathrm{i}a\varphi_{Cm}(a)}{2\pi G_+(\alpha_{Cm})}\int_{-\infty}^{\infty}\frac{\varphi(\alpha,y)}{G_-(\alpha)}\left[\frac{1}{(\alpha-\alpha_{Cm})}-\frac{A(St_\theta)}{(\alpha_{B,\mathrm{gr}}-\alpha_{Cm})}\right]\mathrm{e}^{\mathrm{i}\alpha x}\,\mathrm{d}\alpha - \frac{\mathrm{i}a\varphi^+_{Am}(a)}{2\pi G_+(\alpha^+_{Am})}\int_{-\infty}^{\infty}\frac{\varphi(\alpha,y)}{G_-(\alpha)}\left[\frac{1}{(\alpha-\alpha^+_{Am})}-\frac{A(St_\theta)}{(\alpha_{B,\mathrm{gr}}-\alpha^+_{Am})}\right]\mathrm{e}^{\mathrm{i}\alpha x}\,\mathrm{d}\alpha. \tag{18}$$

The scattering coefficients required for the modelling of the area expansion are then, for scattering of the mth mode in duct A to the nth mode in each of the three duct parts (as defined in the Appendix), given by

$$R^-_{Anm} = \frac{(-1)^m}{G_+(\alpha^+_{Am})G_-(\alpha^-_{An})}\left(\frac{1}{(\alpha^-_{An}-\alpha^+_{Am})}-\frac{A(St_\theta)}{(\alpha_{B,\mathrm{gr}}-\alpha^+_{Am})}\right)F^-_{An}, \tag{19}$$

$$T^+_{BAnm} = \frac{a(-1)^m}{G_+(\alpha^+_{Am})}\left(\frac{1}{(\alpha^+_{Bn}-\alpha^+_{Am})}-\frac{A(St_\theta)}{(\alpha_{B,\mathrm{gr}}-\alpha^+_{Am})}\right)F^+_{Bn}, \tag{20}$$

$$T^-_{CAnm} = \frac{(-1)^m}{G_+(\alpha^+_{Am})G_-(-\alpha_{Cn})}\left(\frac{1}{(\alpha_{Cn}+\alpha^+_{Am})}+\frac{A(St_\theta)}{(\alpha_{B,\mathrm{gr}}-\alpha^+_{Am})}\right)F^-_{Cn}. \tag{21}$$

Second, we have scattering of the mth mode incident from duct C into the nth mode in each duct part,

$$R^-_{Cnm} = -\frac{(-1)^m}{G_+(\alpha_{Cm})G_-(-\alpha_{Cn})}\left(\frac{1}{(\alpha_{Cn}+\alpha_{Cm})}+\frac{A(St_\theta)}{(\alpha_{B,\mathrm{gr}}-\alpha_{Cm})}\right)F^-_{Cn}, \tag{22}$$

$$T^+_{BCnm} = -\frac{a(-1)^m}{G_+(\alpha_{Cm})}\left(\frac{1}{(\alpha^+_{Bn}-\alpha_{Cm})}-\frac{A(St_\theta)}{(\alpha_{B,\mathrm{gr}}-\alpha_{Cm})}\right)F^+_{Bn}, \tag{23}$$

$$T^-_{ACnm} = -\frac{(-1)^m}{G_+(\alpha_{Cm})G_-(\alpha^-_{An})}\left(\frac{1}{(\alpha^-_{An}-\alpha_{Cm})}-\frac{A(St_\theta)}{(\alpha_{B,\mathrm{gr}}-\alpha_{Cm})}\right)F^-_{An}. \tag{24}$$

The functions $F^\pm_{Xn}$ are given in the Appendix.

The reflection coefficient R^- and transmission coefficient T^+ for an area expansion can now be derived from the formulae given in Ref. [1], based on a building block method.

2.2.3. Numerical results

The reflection coefficient is calculated with the unsteady Kutta condition ($A = 0$ in Eq. (16)) and with the relaxed Kutta condition ($A = 1$ in Eq. (16)). Experimental data are taken from Ronneberger [4]. Comparison of the reflection coefficient with experimental results is shown in Figs. 3 and 4. The results show that the original solution, with the unsteady Kutta condition, well represents the experimental data for low Strouhal numbers, as defined in Eq. (2). The solution with the relaxed Kutta condition is valid for large Strouhal numbers where the shear layer is

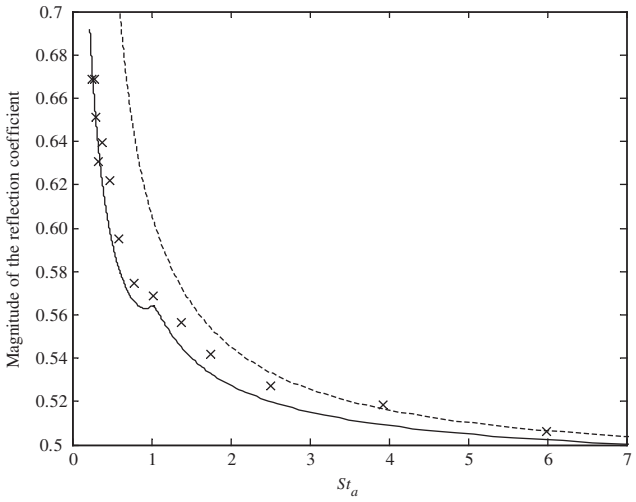

Fig. 3. The plane wave reflection coefficient as a function of the Strouhal number with fixed $ka = 0.11$ and an area expansion ratio of 0.35. '×': experiment [4]; '—' Kutta condition; '...' relaxed Kutta condition.

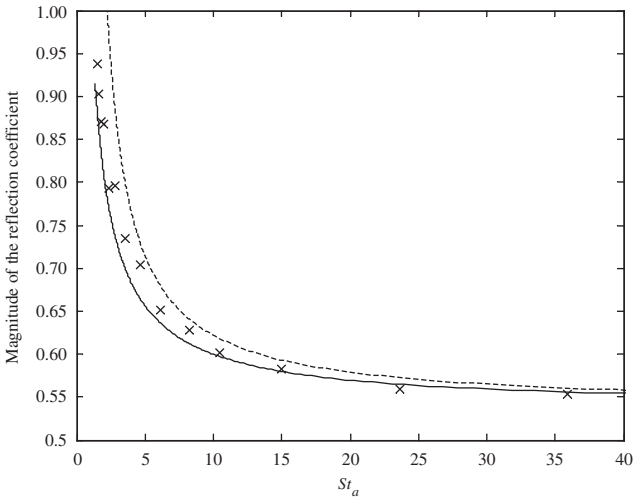

Fig. 4. The plane wave reflection coefficient as a function of the Strouhal number with fixed $ka = 0.67$ and an area expansion ratio of 0.35. '×': experiment [4]; '—' Kutta condition; '...' relaxed Kutta condition.

stable. For intermediate Strouhal numbers, the experimental results are between the model with unsteady Kutta condition (valid for small St_θ) and the model with relaxed Kutta condition (valid for large St_θ), a result expected for the transition region. A rough estimate reveals that the shear layer related to Fig. 3 becomes stable at about $St_a \approx 3.5$. This would correspond to a shear layer Strouhal number of $St_\theta \approx 0.35$, to be compared with values of 0.25 or higher as discussed in Section 2.1.1. The result implies that the model complies with basic physical principles. A proper

adjustment of the coefficient A, which could be based on empirical data, may thus improve the vortex sheet model and extend its validity in the transition region. An alternative method would be to calculate the coefficient A using, e.g., triple-deck theory, as described in Ref. [12] for a wake.

An interesting observation is that the difference between the two solutions gradually decreases as the Strouhal number increases, and the discrepancy to the experimental values is equal for the two solutions. The two models give the same result for large Strouhal numbers, a finding also reported by Howe [13], in comparing a vortex sheet model and a finite width shear layer model. This result indicates that the influence of the hydrodynamic wave decreases as the Strouhal number increases, and that only convective effects persist.

As the difference depending on the edge condition vanishes for large Strouhal numbers, it is mainly in the transition region that the variable edge condition gives an improved model. Studying empirically derived values for A, and the corresponding Strouhal number dependence may also give further insight in to the physics of the coupling between the acoustic field and the shear layer in the transition region.

3. Transmission and absorption at an area expansion

The model that we are studying here is designed with the primary purpose to simulate scattering properties at area expansions followed almost immediately by an area contraction, the area returning to the original. For such a geometry, the assumption of a non-expanding jet is clearly justified. Now, as the model is applied for an area expansion, the validity of the model for this kind of geometry need to be evaluated. The influence from the jet expansion downstream of the area expansion is estimated. As shown in an earlier article [1], the reflection coefficient given by the model agrees well with experimental data. Below, predictions of plane wave transmission and of absorption of acoustic energy are presented together with experimental results, in order to evaluate whether the expansion of the jet has a negligible influence on the plane wave transmission. The calculations are based on the assumption that all the acoustic energy is contained in the plane wave, and that energy contained in hydrodynamic modes can be considered as 'non-acoustic'.

3.1. Plane wave transmission at an area expansion

The scattering model in Ref. [1] presents ways of calculating both reflection and transmission coefficients for sound incident on an area expansion. However, only results for the reflection coefficient are presented there. We will now discuss the results for the transmission coefficient.

The transmission matrix given by the model in Ref. [1] gives the scattering near the area expansion. From a practical point of view it is the sound propagating far downstream of the expansion, where the jet has expanded into a plug flow, that is of interest. In the plane wave region, this propagating part consists of the transmitted plane wave. Our transmission coefficient, though, gives the amplitude of the plane wave in the region upstream of the jet expansion region. Thus, the predicted transmission coefficient does not include any influence from the expansion of the jet.

In fact, for low frequencies it is possible to determine the acoustic field downstream of the jet expansion, neglecting the acoustic interaction with the jet expansion as discussed in Section 2.1.

To show this, the amplitude of the transmitted plane wave is compared with an experimentally measured transmission coefficient [4]. The theoretical results in Figs. 5 and 6 are well in correspondence with the experimental data. Note that there is an experimental value of 0.49 for $M = 0$, corresponding to St equal to infinity.

Concerning the influence of the choice of edge condition, it was found that the effect of relaxed Kutta condition is very small on the transmission coefficient, contrary to the results for the reflection coefficient as discussed in the previous section. Consequently, only computations for the full Kutta condition are presented for the transmission coefficient.

3.2. Absorption

The influence on the sound absorption by the presence of the mean flow field in the flow duct is the next issue to be studied. We want to compare the energy of the incident wave to that of the outward propagating scattered acoustic waves. The latter is assumed to consist of the plane acoustic waves, as only the plane wave region is considered. The main mechanism by which sound is absorbed in this model is through the growing and the attenuated hydrodynamic modes. As their properties (mode shape, phase speed, etc.) differ from those typical of acoustic waves, they are not considered to carry any acoustic energy. Furthermore, the growing hydrodynamic mode is expected to break by nonlinear effects that are not included in the model, the regenerated sound in such a process is assumed to be negligible relative to the incident and scattered sound field.

If the energy of the incident wave is denoted w_{A+}, and that of the outward propagating waves w_{A-} and w_{B+}, respectively, we chose to define the absorption coefficient as

$$\Delta = 1 - (w_{A-} + w_{B+})/w_{A+}. \tag{25}$$

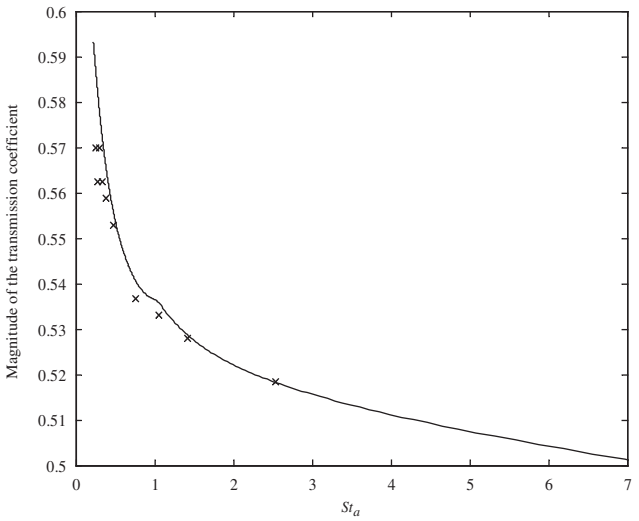

Fig. 5. The plane wave transmission coefficient as a function of the Strouhal number with fixed $ka = 0.11$ and area expansion ratio of 0.35. '×': experiment [4]; '—' theoretical result (full Kutta condition).
N.B., the experimental result $|T| = 0.50$ for $M = 0$, corresponding to $St \to \infty$.

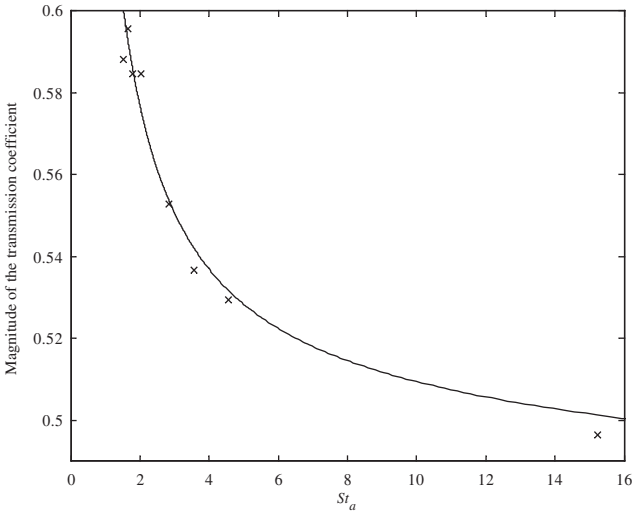

Fig. 6. The plane wave transmission coefficient as a function of the Strouhal number with fixed $ka = 0.67$ and area expansion ratio of 0.35. '×': experiment [4]; '—' theoretical result (full Kutta condition).
N.B., the experimental result $|T| = 0.49$ for $M = 0$, corresponding to $St \to \infty$.

Thus, Δ is the amount of acoustic energy dissipated in the scattering process. Note that other definitions may apply, as the transmitted energy relative to the difference between incident and reflected energy [14].

In the upstream duct, where we have a plug flow, it is straightforward to calculate both incident and reflected sound power. For the energy propagating in the wider duct, there are two options for the definition of the transmitted power. The first option is to calculate the power just downstream of the area expansion. In this region, the jet is not yet expanded, in agreement with the vortex sheet model. However, a complicating fact is that close to the edge, the flow field contains rotational parts. In such a region, there are difficulties in determining the acoustic intensity, both theoretically and experimentally. If the interaction with the expanding jet is indeed negligible, a better alternative would be to evaluate the acoustic intensity in the region where the flow is fully expanded. Results for both these options are presented below.

In general, the intensity in a homentropic flow is defined by [15]

$$\mathbf{I} = (p'/\rho_0 + \mathbf{u}' \cdot \mathbf{U}_0)(\rho_0 \mathbf{u}' + p' \mathbf{U}_0/c^2), \tag{26}$$

and the power through a control volume surface

$$\bar{W} = \iint_S \bar{\mathbf{I}} \cdot \mathrm{d}\mathbf{S}, \tag{27}$$

where the bar indicates the time average. The mean flow is $\mathbf{U}_0 = U_0 \mathbf{e}_x$, and the acoustic particle velocity in the x-direction $u'_x = \mathbf{u}' \cdot \mathbf{e}_x$. Then we can define

$$I_x = (p'/\rho_0 + U u'_x)(\rho_0 u'_x + U p'/c_0^2) \tag{28}$$

for the intensity in the x-direction. If complex quantities are used, we define the pressure as $p' = \mathrm{Re}[\hat{p}e^{-i\omega t}e^{i\alpha_{pl}x}]$ and the acoustic particle velocity as $u'_x = \mathrm{Re}[\hat{u}e^{-i\omega t}e^{i\alpha_{pl}x}]$, where the subscript pl indicates the plane wave. In our case the wavenumbers α_{pl} of the plane waves are real. The intensity can now be expressed as

$$\begin{aligned} I_x &= \frac{1}{2}\mathrm{Re}\left[\left(\frac{\hat{p}}{\rho_0} + U\hat{u}\right)e^{i\alpha_{pl}x}\left\{\left(\rho_0\hat{u} + \frac{\hat{p}}{c_0^2}U\right)e^{i\alpha_{pl}x}\right\}^*\right] \\ &= \frac{1}{2}\mathrm{Re}\left[\left(\frac{\hat{p}}{\rho_0} + U\hat{u}\right)\left\{\left(\rho_0\hat{u} + \frac{\hat{p}}{c_0^2}U\right)\right\}^*\right], \end{aligned} \tag{29}$$

where the stars indicate the complex conjugate. The relation between particle velocity and acoustic pressure is given by the convective momentum equation

$$\rho_0\left(\frac{\partial}{\partial t} + U_0\frac{\partial}{\partial x}\right)\mathbf{u}' = -\nabla p. \tag{30}$$

Fourier transform in time and space yields, $\partial/\partial t \equiv -i\omega$, and $\partial/\partial x \equiv i\alpha$, and in the x-direction we get

$$\rho_0(-i\omega + U_0 i\alpha_{pl})\hat{u} = -i\alpha_{pl}\hat{p}, \tag{31}$$

which finally gives the relation between pressure and velocity as

$$\hat{u} = \frac{\alpha_{pl}}{\rho_0(\omega - U_0\alpha_{pl})}\hat{p} = \frac{\alpha_{pl}}{\rho_0 c_0(k - M\alpha_{pl})}\hat{p}. \tag{32}$$

Using this result, the intensity of a sound wave in a straight duct is

$$I_x(\alpha_{pl}, M) = \frac{|\hat{p}|^2}{2\rho_0 c_0}\left\{M\left(1 + \left|\frac{\alpha_{pl}}{k - M\alpha_{pl}}\right|^2\right) + (1 + M^2)\left(\frac{\alpha_{pl}}{k - M\alpha_{pl}}\right)\right\}. \tag{33}$$

For the uniform velocity profile in duct A, the power in the incident wave is thus given by

$$w_{A+} = I_x(\alpha^+_{A,pl}, M)a, \tag{34}$$

and the power in the reflected wave is

$$w_{A-} = -|R^-|^2 I_x(\alpha^-_{A,pl}, M)a. \tag{35}$$

For the power transmitted into duct B, we present two possible options. Strictly following the vortex sheet model, the power is calculated with the original, non-expanding, velocity profile. This result is compared with that when the transmission coefficient of the vortex sheet model is applied for an expanded flow with constant mean flow speed. The two options correspond to two different control volumes for calculating the absorption, the first is closed near the area expansion excluding the jet expansion, while the second volume includes the jet expansion.

When the power transmitted downstream in duct B is calculated in the region close to the edge where the jet is not expanded, Fig. 2, the resulting expression is

$$w_{B+} = \int_0^b |T^+ \varphi(\alpha^+_{B,\mathrm{pl}}, y)|^2 I_x(\alpha^+_{B,\mathrm{pl}}, M)\,\mathrm{d}y, \tag{36}$$

where $\alpha^+_{B,\mathrm{pl}}$ is the plane wavenumber given by the dispersion relation (3). This integral requires some care, and turns out as

$$\begin{aligned} w_{B+} &= \int_0^b |T^+ \varphi(\alpha^+_{B,\mathrm{pl}}, y)|^2 I_x(\alpha^+_{B,\mathrm{pl}}, M(y))\,\mathrm{d}y \\ &= |T^+|^2 \left(I_x(\alpha^+_{B,\mathrm{pl}}, M) \int_0^a |\varphi(\alpha^+_{B,\mathrm{pl}}, y)|^2\,\mathrm{d}y + I_x(\alpha^+_{B,\mathrm{pl}}, M=0) \int_a^b |\varphi(\alpha^+_{B,\mathrm{pl}}, y)|^2\,\mathrm{d}y \right), \end{aligned} \tag{37}$$

where φ is the mode shape function given in Eq. (4).

With the alternative control volume, the power transmitted downstream in duct B is calculated in the region where, in reality, the flow would be fully expanded (Fig. 2). Then the sound intensity is well defined all across the duct, and the power is given by

$$w_{B+} = |T^+|^2 I_x(\alpha^+_{B,\mathrm{pl,simpl}}, \eta M) b, \tag{38}$$

where $\alpha^+_{B,\mathrm{pl,simpl}} = (1 + M\eta)^{-1}$ and $\eta = a/b$ is the area expansion ratio. The absorption is now given by Eq. (25).

3.2.1. Results

In Fig. 7, the results for the two different control volumes for calculating the absorption coefficient are compared with experimental data [4]. As expected, the experimental data is best reproduced when the control volume includes the region where the flow is expanded. Furthermore, the agreement between theoretical and experimental data is excellent, an additional argument for the vortex sheet model.

The Strouhal number is varied by varying the Mach number for a fixed Helmholtz number ka. Above $St = 1$, the absorption decreases very slowly, whereas below $St = 1$, it increases rapidly with decreasing Strouhal number (increasing M). Note that the model is restricted to subsonic Mach numbers. This sets a limit to how small the Strouhal number can be for a specific Helmholtz number.

4. Summary and conclusions

The analytical, full mode model for scattering of sound encountering an area expansion in a flow duct as presented by Boij and Nilsson [1] is evaluated. Two different aspects are studied. Of particular interest is to investigate the influence of the flow field on the acoustic scattering. First, the influence on reflection of the edge condition applied at the edge is discussed. Then the applicability of the model concerning results for transmission properties, and influence of the jet expansion is investigated.

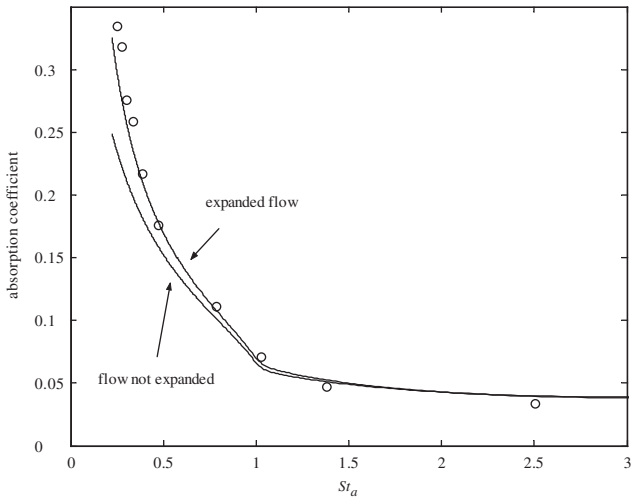

Fig. 7. The absorption coefficient, Eq. (25), as a function of the Strouhal number ka/M, $ka = 0.11$ and area expansion ratio of 0.35. '○' experiment [4], Theoretical results: '—' transmitted power given by Eq. (36), '...' transmitted power given by Eq. (38).

In the model, the flow field downstream of the expansion is a non-expanding jet, a vortex sheet separating the moving and the quiescent fluid. The instability of such a vortex sheet, as reported by Michalke [8] for instance, is a small Strouhal number phenomenon. A method to avoid the excitation of the instability of the shear layer in the model, and thus extend the applicable Strouhal number range of the model, is presented in Section 2. This is done by suppressing the unstable part of the solution, a growing hydrodynamic wave. The suppression is achieved by changing the unsteady Kutta condition applied at the edge. A region where the variable edge condition may improve the correspondence between theory and experiment for the reflection can be observed around the critical Strouhal numbers for the stability of the shear layer reported by Freymuth [6] and Michalke [8]. At even higher Strouhal number, the two solutions seem to converge, a behaviour also reported by Howe [13]. This is an interesting observation, indicating that the importance of the hydrodynamic modes is reduced for large Strouhal numbers. The vortex sheet model for scattering at an open flow duct termination by Munt [16] also shows good agreement with experimental data when the shear layer has a non-negligible thickness.

In order to evaluate the transmission properties given by the model, the plane wave transmission coefficient and sound absorption are compared with experimental data. It is of interest to see whether the model is applicable to an area expansion, regardless of the fact that the jet expansion region is missing in the model. Calculation of the transmission coefficient is presented in Section 3. A comparison of the transmission coefficient of the model [1] with experimental results [4], shows good agreement. It is also observed, in contrast to results for reflection, that for the transmission coefficient the difference between the two versions of the Kutta condition is very small.

The absorption of acoustic energy due to the interaction with the flow is calculated using the standard definition of sound intensity in moving media, Section 3. The absorption is calculated

both excluding and including the region of flow expansion. When the absorption based on the experimental results is calculated, the theoretical absorption including the expansion region agrees well with these results. Thus, it supports the idea that the interaction between the acoustic field and the vortex shedding at the edge is responsible for most of the absorption.

Now, we have two interesting results concerning the Strouhal number dependence of the coupling between the acoustic field and the flow field, the latter represented in part by the hydrodynamic waves in the vortex sheet model. Considering the importance of the coupling to the hydrodynamic wave in the scattering process, Section 2, this coupling seems to have little importance for large Strouhal numbers. For the case of absorption, Section 3, the amount of acoustic energy dissipated to the flow field has a different Strouhal number dependence for small and large Strouhal numbers, respectively. For large St, it varies very slowly but for small St it increases rapidly with decreasing St. These two observations indicate that the hydrodynamic wave has less influence for St larger than some critical value. This value turns out to coincide with the St where the first higher order mode becomes less damped than the hydrodynamic mode, and when the mode shapes of these start to be concentrated to the vortex sheet. For mode shapes, please consult [5]. A small peak can be seen at this Strouhal number in the curves for the reflection and transmission coefficients. It is a phenomenon inherent in the model, and does not originate from any numerical problems. A preliminary investigation shows that it is related to the interaction between the hydrodynamic modes and the first higher order acoustic mode, corresponding to a particularly strong coupling at the point of flow separation. This phenomenon is further studied in Ref. [17].

In all, predictions by the vortex sheet model agree well with measurement data [4]. The close agreement between theory and experiment gives support for the vortex sheet model. It includes the main coupling between the flow and the sound in the plane wave region. Improvements are found in including the stability properties of the shear layer. In the frequency region considered in this paper, this effect is shown to be more important than the back scattering due to turbulence in the jet expansion region. These results strongly support the assumption that the interaction between the flow and the sound field occurs mainly at the edge, and that the interaction is mainly governed by the stability properties of the shear layer.

Appendix

In ducts A and C, the wavenumbers α and mode φ shapes for the nth mode are, assuming a harmonic time dependence $\exp(-\mathrm{i}\omega t)$,

$$\alpha_{An}^{\pm} = -\frac{kM}{(1-M^2)} \pm \frac{\sqrt{k^2-(1-M^2)(n\pi/a)^2}}{(1-M^2)}, \quad n = 0, 1, 2, \ldots, \tag{39}$$

$$\varphi_{An}(y) = \cos(n\pi y/a), \tag{40}$$

$$\pm\alpha_{Cn} \equiv \alpha_{Cn}^{\pm} = \pm\sqrt{k^2-(n\pi/c)^2}, \quad n = 0, 1, 2, \ldots, \tag{41}$$

$$\varphi_{Cn}(y) = \cos(n\pi(b-y)/c), \tag{42}$$

where $k = \omega/c_0$ is the wavenumber and a, b and c are the widths of ducts A–C. The square root is defined so that it has a positive imaginary part. In duct B, no explicit expression is found for the wavenumbers $\alpha_{Bn}^{\pm}$, but they are solutions to the dispersion relation, Eq. (3). Let $H_{Bn}^{\pm}$ and $h_{Bn}^{\pm}$ denote H and h when $\alpha = \alpha_{Bn}^{\pm}$. The mode shape for the nth mode in duct B is

$$\varphi(\alpha_{Bn}^{\pm}, y) = \varphi_{Bn}^{\pm}(y) = \frac{1}{N(\alpha_{Bn}^{\pm})} \begin{cases} -\dfrac{(1 - M\alpha_{Bn}^{\pm}/k)^2}{H_{Bn}^{\pm} a \sin H_{Bn}^{\pm} a} \cos H_{Bn}^{\pm} y, & 0 < y < a, \\ \dfrac{1}{h_{Bn}^{\pm} a \sin h_{Bn}^{\pm} c} \cos h_{Bn}^{\pm}(b - y), & a < y < b, \end{cases} \tag{43}$$

where the mode shape is normalised so that the mean value of φ across the duct is one, thus

$$N(\alpha) = \frac{a}{b} \frac{M\alpha^3(M\alpha - 2k)}{(ka)^2(k^2 - \alpha^2)((k - M\alpha)^2 - \alpha^2)}. \tag{44}$$

The functions G_+ and G_- are infinite products containing the wavenumbers, defined as

$$G_+(\alpha) = \frac{(1 - \alpha/\alpha_{B,\mathrm{pl}}^-)}{(1 - \alpha/\alpha_{A,\mathrm{pl}}^-)(1 - \alpha/\alpha_{C,\mathrm{pl}}^-)} M_+(\alpha)\sqrt{G(0)}, \tag{45}$$

and

$$G_-(\alpha) = \frac{(1 - \alpha/\alpha_{B,\mathrm{gr}}^+)(1 - \alpha/\alpha_{B,\mathrm{da}}^+)(1 - \alpha/\alpha_{B,\mathrm{pl}}^+)}{(1 - \alpha/\alpha_{A,\mathrm{pl}}^+)(1 - \alpha/\alpha_{C,\mathrm{pl}}^+)} M_-(\alpha)\sqrt{G(0)}, \tag{46}$$

where the subscript pl indicates the wavenumber of the plane wave, subscript gr indicates the growing hydrodynamic mode and subscript da the damped hydrodynamic mode. The factors M incorporate an infinite product involving all higher order acoustic modes

$$M_{\pm}(\alpha) = \prod_{n=3}^{\infty} \frac{(1 - \alpha/\alpha_{Bn}^{\mp})}{(1 - \alpha/\alpha_{An}^{\mp})(1 - \alpha/\alpha_{Cn}^{\mp})}. \tag{47}$$

The functions $F_{\mathrm{X}n}^{\pm}$ are given by

$$F_{An}^- = \frac{(-1)^{n+1}(1 - M\alpha_{An}^-/k)^2}{(1 + \delta_{m0})a[(1 - M^2)\alpha_{An}^- + Mk]},$$

$$F_{Bn}^+ = N(\alpha_{Bn}^+) \operatorname*{Res}_{\alpha = \alpha_{Bn}^+} \left[\frac{1}{G_-(\alpha)}\right],$$

$$F_{Cn}^- = \frac{(-1)^n}{(1 + \delta_{n0})c\alpha_{Cn}},$$

where δ_{n0} is the Kronecker delta.

References

[1] S. Boij, B. Nilsson, Reflection of sound at area expansions in a flow duct, *Journal of Sound and Vibration* 260 (2003) 477–498.
[2] D.G. Crighton, The Kutta condition in unsteady flow, *Annual Review of Fluid Mechanics* 17 (1985) 411–445.
[3] G.K. Batchelor, *An Introduction to Fluid Dynamics*, Cambridge University Press, Cambridge, 1967.
[4] D. Ronneberger, *Theoretische und experimentelle Untersuchung der Schallausbreitung durch Querschnittssprünge und Lochplatten in Strömungskanälen*, DFG-Abschlussbericht, Drittes Physikalisches Institut der Universität Göttingen, 1987.
[5] B. Nilsson, Scattering of stable and unstable waves in a flow duct, *Quarterly Journal of Mechanics and Applied Mathematics* 51 (1998) 599–632.
[6] P. Freymuth, On transition in a separated boundary layer, *Journal of Fluid Mechanics* 25 (1966) 683–704.
[7] D.S. Jones, The scattering of sound by a simple shear layer, *Philosophical Transactions of the Royal Society A* 284 (1977) 287–328.
[8] A. Michalke, On spatially growing disturbances in an inviscid shear layer, *Journal of Fluid Mechanics* 23 (1965) 521–544.
[9] F.W. Chambers, V.W. Goldschmidt, Acoustic interaction with a turbulent plane jet: effects on mean flow, *AIAA Journal* 20 (1982) 797–804.
[10] M. Åbom, B. Nilsson, Sound transmission at a sudden area expansion in a flow duct, *Proceedings of the 15th International Congress of Acoustics, Trondheim, Norway*, 1995.
[11] B. Noble, *Methods Based on the Wiener–Hopf Technique*, Chelsea Publishing Company, New York, 1958.
[12] S.W. Rienstra, Sound diffracted at a trailing edge, *Journal of Fluid Mechanics* 108 (1981) 443–460.
[13] M.S. Howe, Attenuation of sound in a low Mach number nozzle flow, *Journal of Fluid Mechanics* 91 (1979) 209–229.
[14] D.W. Bechert, Sound absorption caused by vorticity shedding, demonstrated with a jet flow, *Journal of Sound and Vibration* 70 (1980) 389–405.
[15] M.K. Myers, Transport of energy by disturbances in arbitrary steady flows, *Journal of Fluid Mechanics* 226 (1991) 383–400.
[16] R.M. Munt, Acoustic transmission properties of a jet pipe with subsonic jet flow: I. The cold jet reflection coefficient, *Journal of Sound and Vibration* 142 (1990) 413–436.
[17] S. Boij, Acoustic Scattering in Ducts and Influence of Flow Coupling, Ph.D. thesis, Royal Institute of Technology, Stockholm, 2003.